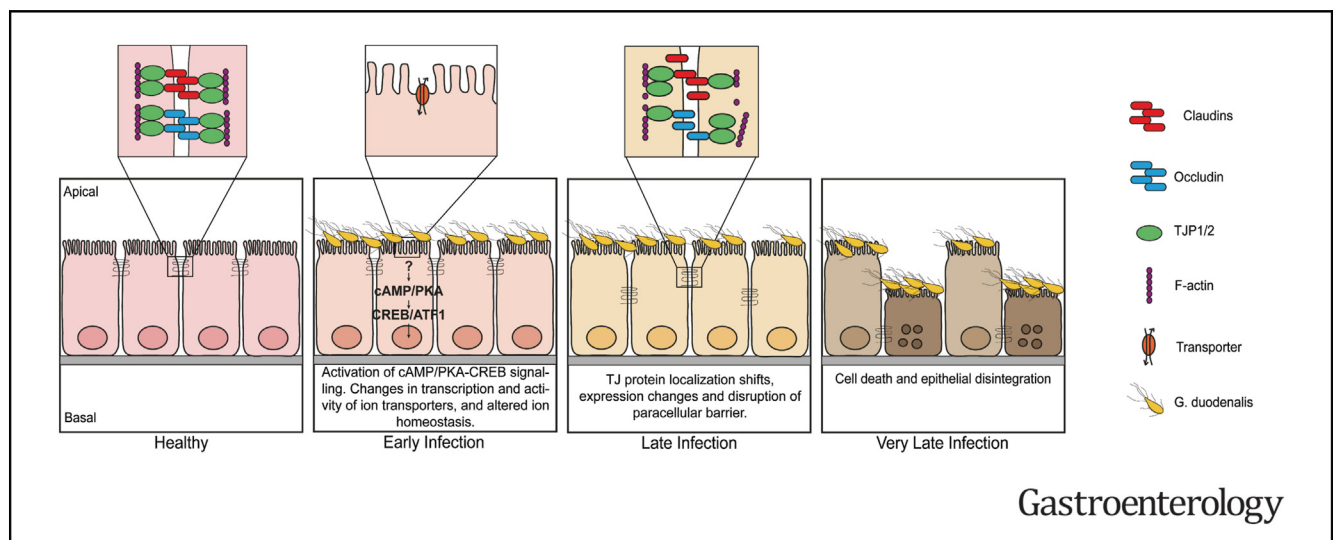# Dissection of Barrier Dysfunction in Organoid-Derived Human Intestinal Epithelia Induced by *Giardia duodenalis*

David Holthaus,[1,*] **Martin R. Kraft**,[1,*] Susanne M. Krug,[2] Silver Wolf,[3] Antonia Müller,[1] Estefania Delgado Betancourt,[1] Madeleine Schorr,[4] Gudrun Holland,[5] Felix Knauf,[4] Joerg-Dieter Schulzke,[2] Toni Aebischer,[1,§] and Christian Klotz[1,§]

[1]Department of Infectious Diseases, Unit 16 Mycotic and Parasitic Agents and Mycobacteria, Robert Koch-Institute, Berlin, Germany; [2]Department of Gastroenterology, Rheumatology and Infectious Diseases, Clinical Physiology Nutritional Medicine, Charité-Universitätsmedizin Berlin, Berlin, Germany; [3]MF 1 Bioinformatics, Robert Koch-Institute, Berlin, Germany; [4]Department of Nephrology and Medical Intensive Care, Charité-Universitätsmedizin Berlin, Berlin, Germany; and [5]Advanced Light and Electron Microscopy, Centre for Biological Threats and Special Pathogens, Robert Koch-Institute, Berlin, Germany

BACKGROUND & AIMS: The protozoa *Giardia duodenalis* is a major cause of gastrointestinal illness worldwide, but underlying pathophysiological mechanisms remain obscure, partly due to the absence of adequate cellular models. We aimed at overcoming these limitations and recapitulating the authentic series of pathogenic events in the primary human duodenal tissue by using the human organoid system. **METHODS:** We established a compartmentalized cellular transwell system with electrophysiological and barrier properties akin to duodenal mucosa and dissected the events leading to *G. duodenalis*-induced barrier breakdown by functional analysis of transcriptional, electrophysiological, and tight junction components. **RESULTS:** Organoid-derived cell layers of different donors showed a time- and parasite load-dependent leak flux indicated by collapse of the epithelial barrier upon *G. duodenalis* infection. Gene set enrichment analysis suggested major expression changes, including gene sets contributing to ion transport and tight junction structure. Solute carrier family 12 member 2 and cystic fibrosis transmembrane conductance regulator-dependent chloride secretion was reduced early after infection, while changes in the tight junction composition, localization, and structural organization occurred later as revealed by immunofluorescence analysis and freeze fracture electron microscopy. Functionally, barrier loss was linked to the adenosine 3′,5′-cyclic monophosphate (cAMP)/protein kinase A-cAMP response element-binding protein signaling pathway. **CONCLUSIONS:** Data suggest a previously unknown sequence of events culminating in intestinal barrier dysfunction upon *G. duodenalis* infection during which alterations of cellular ion transport were followed by breakdown of the tight junctional complex and loss of epithelial integrity, events involving a cAMP/protein kinase A-cAMP response element-binding protein mechanism. These findings and the newly established organoid-derived model to study *G. duodenalis* infection may help to explore new options for intervening with disease and infection, in particular relevant for chronic cases of giardiasis.

P rotozoan parasites *Giardia duodenalis* (synonym *G. lamblia* and *G. intestinalis;* further referred to as *Giardia*) cause the gastrointestinal disease giardiasis.[1] It is one of the most prevalent parasitic diseases worldwide with ∼183 million symptomatic cases each year.[2] Disease mechanisms in humans are not understood, partly due to the lack of adequate model systems.

The clinical outcome varies and ranges from asymptomatic colonization to severe acute or chronic disease. It is thought to reflect a complex interaction of *Giardia* parasites with the host epithelium, modulated by local microbiome and dietary factors.[1,3] Common symptoms are malabsorption, diarrhea, bloating, abdominal pain, nausea, and other gastrointestinal complaints.[1] Long-term sequelae reportedly linked to infection are stunting (in pediatric patients) and irritable bowel and chronic fatigue syndromes.[1]

Only a few studies have reported histologic correlates of infection in asymptomatic and symptomatic, acute or chronic disease. In a large case series of 567 adult patients undergoing endoscopy because of unspecific gastrointestinal complaints, giardiasis was diagnosed based on parasites found in biopsy specimens primarily in the duodenum and distributed along the crypt to villus tip axis.[4,5] There, an inflammatory reaction was detected in less than 4% of cases, while the mucosa seemed unaffected in most patients, despite 32% of them experiencing diarrhea.[4] Moreover, a study of 13 patients with chronic symptomatic giardiasis detected inflammatory cells, a 50% reduction of villous surface, and decreased electrical resistance of mucosal biopsy specimens, indicating compromised absorptive and barrier properties of the epithelium.[6]

To date, attempts to reproduce these in vivo findings in vitro depended on the use of immortalized cancer cell lines as substitutes of intestinal epithelia to decipher molecular mechanisms but have yielded highly conflicting results.[1,7] Common cell line models, such as the colon carcinoma-derived Caco-2 cells, are further limited by the imprint on gene expression of their origin, the colon,[8,9] which differs, for example, in tight junction (TJ) composition from the small intestine. Moreover, the cell lines do not tolerate well media that maintain best *Giardia*'s fitness.[10] All of these reasons compromise the use of cell lines as a translational model to investigate *Giardia* infection. The recent development of small intestinal stem cell-derived primary organoids promises desirable improvement,[11] in particular, since inflammation as stated above, appears not conditional for disease.

In this study, we established a reliable in vitro system based on such organoids to decipher the effects of *Giardia* infection on barrier function in human primary tissue under conditions that preserve *Giardia* viability. This enabled via transcriptomic, functional, and structural analyses the elucidation of a parasite-induced cascade of events implicating adenosine 3′,5′-cyclic monophosphate (cAMP)/

WHAT YOU NEED TO KNOW

BACKGROUND AND CONTEXT

Cell lines may fail to reproduce epithelia-directed pathogenic events of human *Giardia duodenalis* infections. Thus, intestinal stem cell-derived primary epithelia were used for interaction studies of this pathogen as its target tissue.

NEW FINDINGS

Events involving early adenosine 3′,5′-cyclic monophosphate-protein kinase A-adenosine 3′,5′-cyclic monophosphate response element-binding protein signaling, followed by reduced ion transporter expression/activity and functionally linked to altered make and function of tight junctions lead to loss of barrier function and cell apoptosis.

LIMITATIONS

Although based on primary epithelia the model lacks parts of the intestinal target tissue such as subepithelial immune cells and luminal microbiota.

IMPACT

The tractable intestinal organoid-derived primary cell system to study *Giardia duodenalis* infections demonstrates suitability to gain mechanistic insight with potential to instruct new avenues to mitigate symptomatic infections.

---

protein kinase A (PKA) signaling in the lead up to barrier breakdown.

Materials and Methods

For detailed descriptions of methods and reagents see the Supplementary Methods and Supplementary Tables 1 and 2 online.

Organoid Culture

Human organoids were generated and maintained from duodenal biopsy specimens from healthy volunteers undergoing routine examinations at Charité-Universitätmedizin Berlin (ethics approval #EA4-015-13 by local authorities) as described (Supplementary Methods).[12,13]

Organoid-derived monolayers (ODMs) were prepared on Matrigel-coated (Corning, Tewksbury, NY) transwell cell culture

* Authors share co-first authorship; § Authors share co-senior authorship.

Most current article

inserts (0.6 cm^2, 0.4-μm pores; Merck-Millipore, Burlington, MA). For this, organoids were harvested in ice-cold Advanced Dulbecco's modified Eagle medium/F12, centrifuged, and mechanically disrupted as described for passaging. Cells were sedimented, resuspended in differentiation medium (organoid medium without WRN-conditioned medium, A83-01, and SB202190), and added to the apical compartment of the insert. Differentiation medium was applied to both compartments of the transwell system and exchanged every 2 to 3 days. For the first 2 days, 10 μmol/L Y-27632 was added to inhibit anoikis.

Parasite Culture

Giardia WB6 (ATCC 50803) trophozoites were cultured at 37°C in flat-sided 10-mL tubes (Nunclon; Thermo Scientific, Waltham, MA) in Keister's modified TYI-S-33 medium,[14] supplemented with 10% adult bovine serum (Gibco, Grand Island, NY), 100 μg/mL streptomycin/100 U/mL penicillin (Capricorn, Frederick, MD), and 0.05% bovine/ovine bile (Sigma-Aldrich, St. Louis, MO). Trophozoites were passaged the day before infection experiments to guarantee logarithmic growth phase. For passaging, culture tubes were chilled on ice for 20 minutes to detach trophozoites. Parasites were quantified using a Neubauer counting chamber. For infection, detached parasites were pelleted at 1000g for 5 minutes at 4°C and suspended according to desired concentration in complete TYI-S-33 medium.

Infection of Organoid-Derived Monolayers

Apical compartment medium of 8- to 10-day-old ODMs was replaced with complete TYI-S-33 the evening before infection to adapt cells to the TYI-S-33 medium. Medium was renewed before infection (ie, TYI-S-33 in the apical and organoid differentiation medium in the basal compartment). *Giardia* trophozoites were added apically. For experiments with parasite lysates, trophozoites were sonicated for 10 minutes at 4°C (30 seconds on/off; power 72-D) with a 450 Digital Sonifier (Branson, Brookfield, CT) and added to monolayers as indicated.

Transepithelial Electric Resistance Measurements

Transepithelial electric resistance (TEER) measurements were conducted on a 37°C heating block using a Millicell ERS-2 Voltohmmeter (Merck-Millipore) equipped with a Ag/AgCl electrode (STX01; Merck-Millipore). Blank electric resistance (cell-free transwell insert) was subtracted from raw resistance values and standardized for 1 cm^2 surface area.

To test the effect of chemical compounds and recombinant human tumor necrosis factor (TNF)-α (PeproTech, Cranbury, NJ) on TEER, the substances were added to the ODMs the evening before infection to allow sufficient preincubation time, except for staurosporine, H89, cAMP, E64d, 3-isobutyl-1-methylxanthine, and HLM006474. All substances were added to both compartments, except for staurosporine and E64d, which were added to the apical compartment only. Substances were renewed every 24 hours, except for staurosporine. The following concentrations of inhibitors were used in all respective experiments: 10 μmol/L H89-dihydrochloride (PKA inhibitor; Merck), 1 mmol/L dibutyl (db)-cAMP (PeproTech), 40 μmol/L Z-DEVD-FMK (caspase 3-inhibitor; BD Biosciences, San Jose, CA), 40 μmol/L Z-VAD(OMe)-FMK (pan-caspase inhibitor; Cayman Chemical, Ann Arbor, MI), 40 μmol/L ML-9 (myosin light-chain kinase [MLCK] inhibitor; Cayman Chemical), 20 μmol/L ML-7 hydrochloride (MLCK-inhibitor; Cayman Chemical), 1 to 2 μmol/L staurosporine (induces nonselectively apoptosis; Tocris, Bristol, United Kingdom), 10 μmol/L E64d (cysteine protease inhibitor; Carl Roth, Karlsruhe, Germany), 1 mmol/L 3-isobutyl-1-methylxanthine (cAMP phosphodiesterase inhibitor; Thermo Scientific), and 50 μmol/L HLM006474 (E2F modulator; Merck).

Dilution Potential Measurements

Dilution potential measurements to determine permeabilities for Na$^+$ and Cl$^-$ were performed in Ussing chambers modified for cell-culture inserts. Water-jacketed gas lifts kept at 37°C were filled with 10 mL bathing solution that contained (in mmol/L) 119 NaCl, 21 NaHCO$_3$, 5.4 KCl, 1.2 CaCl$_2$, 1 MgSO$_4$, 3 HEPES, and 10 D(+)-glucose, and was gassed with 95% O$_2$ and 5% CO$_2$, resulting in a pH of 7.4. Data were corrected for resistance of empty filters and bathing solution. Dilution potentials were measured replacing half of NaCl by mannitol on apical or basolateral sides. P_{Na} and P_{Cl} ratios and Na$^+$ and Cl$^-$ absolute permeabilities were calculated using the Goldman-Hodgkin-Katz equation.[15]

Short-Circuit Current and Ion Secretion/Transport via Solute Carrier Family 12 Member 2 and Cystic Fibrosis Transmembrane Conductance Regulator

Net ion transport was determined by measurement of changes in short-circuit current (I_{SC}) until steady state. Secretion of Cl$^-$ was stimulated with prostaglandin E$_2$ (1 μmol/L, basal side) and theophylline (10 mmol/L, both sides). The effect of both was antagonized by bumetanide (10 μmol/L, basal side) inhibition of solute carrier family 12 member 2 (SLC12A2, Na-K-Cl cotransporter 1 [NKCC1]), and ΔI_{SC} was derived by comparison of both conditions. Cystic fibrosis transmembrane conductance regulator (CFTR) activity was determined by stimulating Cl$^-$ secretion by 10 μmol/L forskolin, inhibiting CFTR then with 10 μmol/L 5-nitro-2-(3-phenylpropylamino) benzoic acid (NPPB) and stimulating again to derive noninhibitable fractions.

Fluorescein and Fluorescein Isothiocyanate-Dextran Flux Assay

Fluxes of fluorescein (332 Da) and fluorescein isothiocyanate-dextran 4 (FD4, ∼4000 Da) were determined in Ussing chambers under short-circuit conditions. Fluorescein was added apically (0.1 mmol/L), and basal samples were taken at 0, 10, 20, 30, and 40 minutes. For FD4 fluxes, dialyzed FD4 (0.04 mmol/L) was added apically and basolaterally counterbalanced with unlabeled dextran of the same concentration. Basal samples were taken at 0, 20, 40, 60, and 80 minutes. Fluxes and apparent permeabilities were calculated based on fluorometric readings of the respective concentrations.

Results

A Human Two-Dimensional Primary Intestinal Epithelium Suitable to Model Giardia Infections

A suitable model to study the effects of *Giardia* on barrier function of human primary duodenal epithelial cells

should fulfill the following criteria: (1) apical and basolateral compartments separated by a polarized columnar cell layer for individual manipulation, and (2) electrophysiological and barrier properties akin to a duodenal epithelium.

Using 3-dimensional stem cell-enriched organoid cultures from human duodenal biopsy specimens, we set-up a 2-dimensional transwell system, referred to as organoid-derived monolayers (ODM, see the Supplementary Methods for details).[12,13] ODMs reproducibly showed increasing TEER values that leveled at $\sim 250 \, \Omega \cdot cm^2$ after 9 days of culture (Figure 1*A*). At this time point, mRNA and immunofluorescence analyses showed enrichment for markers of enterocyte/absorptive cells (Figure 1*B*, Supplementary Figure S1). ODMs reached a height of ~ 20 μm, and cells demonstrated the typical polarized enterocyte-like shape with microvilli and well-developed cellular junctions (Figure 1*B–D*, Supplementary Figure S1). The cells expressed enterocytes' hallmarks such as apically a functional sodium–glucose cotransporter 1, transcribed apolipoprotein B (APOB) mRNA editing enzyme catalytic subunit 1 (*APOBEC1*) and APOBEC1 complementation factor (*A1CF*) required for APOB mRNA editing, and translated enterocyte-specific APOB-48 protein required for chylomicron formation (Figure 1*E–G*). Accumulation of lipid droplets in cells exposed apically to oleic acid (Supplementary Figure S2) indicated apical lipid absorption capabilities. Altogether, this implied establishment of a tight epithelial barrier primarily composed of enterocyte-type cells, the dominant cell type of the natural duodenal epithelium.

Infection of Organoid-Derived Monolayers With Giardia *Leads to Barrier Breakdown*

For in vitro growth, *Giardia* as a microaerophilic organism requires highly reducing growth media such as Keisters' modified TYI-S-33, which contains bile acids to better mimic duodenal conditions. This medium was found to be toxic to cell lines such as Caco-2, and therefore, interaction studies on *Giardia* infection required use of medium mixtures or used pure Dulbecco's modified Eagle medium.[7,10] In contrast, ODM exposed to TYI-S-33 in the apical compartment of the transwell system and organoid differentiation medium basolaterally after equilibration showed stable TEER for at least 3 days (Figure 2*A* and *B*). These conditions were used for subsequent experiments.

To study effects of *Giardia* on barrier function, ODMs were infected with trophozoites at multiplicities of infection (MOI) ranging from 1 to 10, roughly saturating the ODM surface at MOI 10 (Figure 2*A*, Supplementary Figure S3). TEER started to decrease dose- and time-dependently after 24 hours of infection (Figure 2*B*). This loss of TEER was reproducibly observed when infecting ODMs established from several individual donors (Supplementary Figure S4). We also tested the effect of various *Giardia* genotypes on TEER at MOI 10 and found a similar pattern of TEER decrease after infection (Supplementary Figure S5). Paracellular barrier changes were further probed with fluorescein (332 Da) and FD4 ($\sim$4000 Da). In line with TEER

decreasing, exclusion of apical fluorescein and FD4 from the lower compartment was compromised in a MOI- and time-dependent manner (Figure 2*C* and *D*), indicating that not only permeabilities for ions and small solutes were affected but also permeability for macromolecules. The observed changes furthermore were suggesting an overall decrease and final loss of barrier properties.

Using conventional epithelial cell line models, discordant observations had been reported on paracellular barrier and TEER breakdown due to *Giardia*, but when observed, they had been linked to parasite-released cysteine protease activity and activation of caspase-3–dependent apoptosis of the cells.[1,16,17] Caspase-3–dependent processes reported could be inhibited by MLCK inhibitors.[18] Therefore, we tested whether TEER decrease in infected ODMs would proceed by cysteine protease triggered, MLCK-mediated apoptosis. First, apoptosis of infected ODMs was assessed by terminal deoxynucleotidyl transferase–mediated deoxyuridine triphosphate nick-end labeling (TUNEL) staining 24, 48, and 72 hours after infection. Elevated numbers of TUNEL-positive cells were observable but only after 48 hours infection at MOI 10 and at 72 hours at MOI 5 and 10. Also, apoptotic cell frequency rose to $\sim$6% only, which was just a fraction of the staurosporine-induced apoptotic cell number in controls (Figure 2*E*). Thus, elevated apoptosis rates could only be observed after TEER breakdown had occurred. In line, addition of inhibitors of MLCK (ML-7 or ML-9) or caspases (pan-caspase and caspase-3 inhibitors) (Figure 2*F*, Supplementary Figure S6) had no effect.

To analyze the role reported for parasite cysteine proteinases,[1,17] ODMs were incubated with parasite lysates corresponding to the MOI range used above. Unexpectedly, this did not cause TEER decline (Figure 2*F*) despite high cysteine protease activity (Supplementary Figure S7). Inhibition of cysteine proteases by E64d did also not prevent parasite-induced TEER breakdown (Figure 2*F*). To test for possibly decreased parasite fitness during assays, we excluded that trophozoite viability was altered in the test interval (Supplementary Figure S8).

Giardia *Infection of Organoid-Derived Monolayers Induces Transcriptional Responses in Pathways for Cell Cycle Control, Cell-Autonomous Innate Immune Response, Ion Transport, and TJ Structure*

To discover early responses that may precede and cause TEER changes and barrier breakdown, we performed a transcriptome analysis at time points after infection, but before TEER decline. ODMs were exposed to *Giardia* or control treatment and harvested after 1.5 and 24 hours for RNA sequencing analysis. Principle component analysis of mRNA changes in samples analyzed 1.5 hours after infection indicated no significant effect compared with noninfected controls (Figure 3*A*). In contrast, transcriptomes changed reproducibly in the 5 infected biological replicates at 24 hours (Figure 3*A* and *B*). Analysis of protein-encoding mRNAs revealed 917 significantly more and 604 less

abundant transcripts 24 hours after infection of 14,727 protein-coding genes analyzed (Figure 3C, Supplementary Data File 1).

Next, gene set enrichment analysis (GSEA)[19] with subsequent leading edge and network analysis of enriched gene sets was performed. GSEA of 50 "Hallmark" gene sets
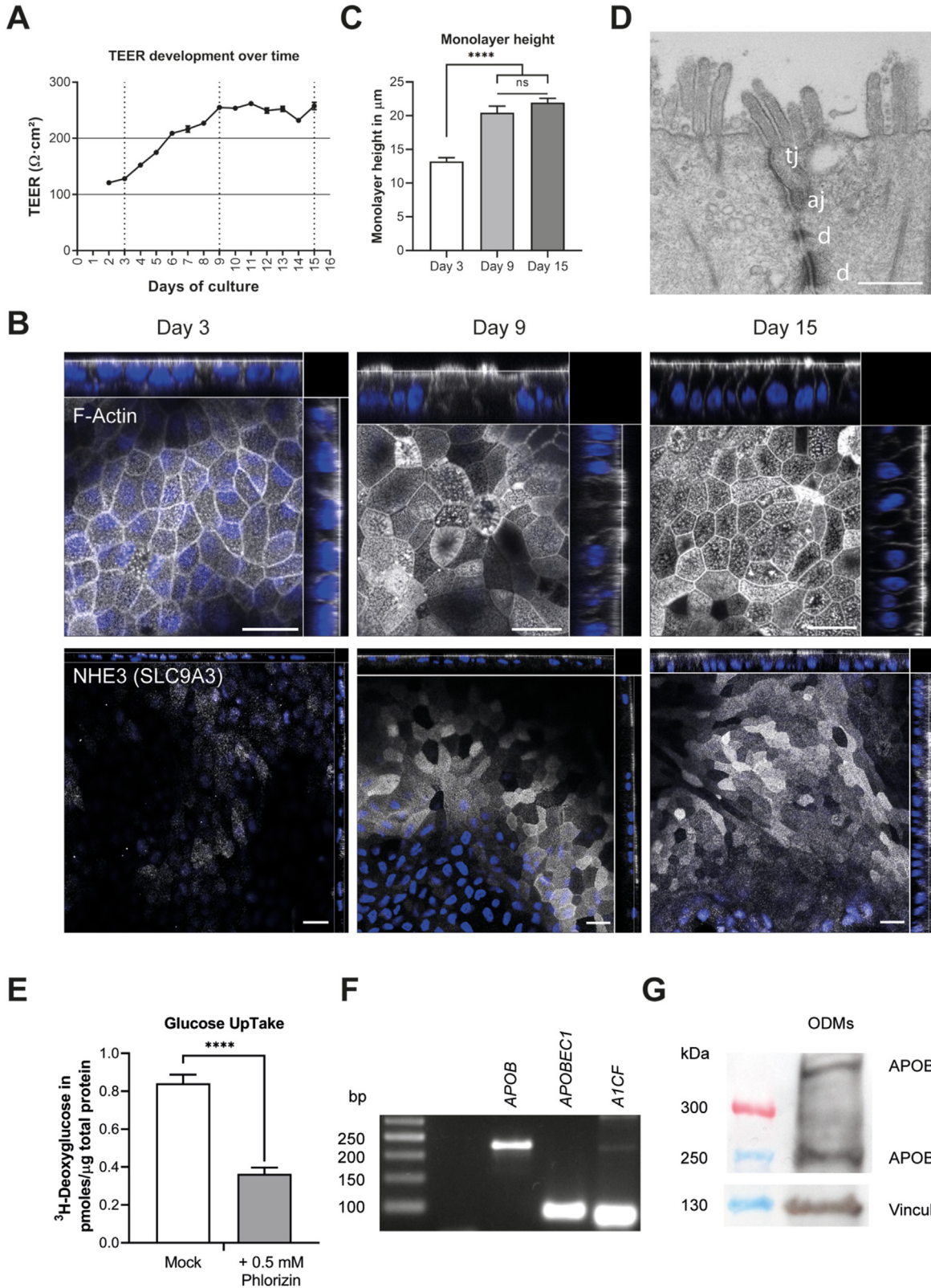
encompassing well-defined biological processes indicated signatures for epithelial cells' innate immune response, including TNF-α via NF-κB signaling (Figure 3D, Supplementary Table 3). Furthermore, gene sets representing apical junction biology, apoptosis and stress responses (UV-treatment and hypoxia response-related genes) were highly enriched. In contrast, mRNAs corresponding to sets of genes involved in cell cycle, DNA replication, and cell growth were reduced after *Giardia* infection (Figure 3D, Supplementary Table 3).

For probing potential functional connectivity in the transcriptional response, a network analysis of enriched gene sets was performed based on a curated collection comprising 1612 gene sets representing distinct pathways and stimuli-specific responses. The analysis was consistent with the hallmark GSEA but, in addition, suggested a likely correspondence between reduced cell cycle and DNA-repair activity, increased nuclear receptor signaling and decreased nuclear transport, as well as RNA processing and a general negative effect on expression of genes in a gene set for solute and ion transport (Figure 3E and F).

For aspects like epithelial cells' innate immune reaction (NF-κB pathway and chemokine upregulation) and cell cycle arrest, data are congruent with previous studies using Caco-2.[20,21] The respective response of Caco-2 cells was faster and of larger amplitude. In contrast, mRNA transcripts encoding TJ proteins, proteins involved in response to oxidative stress and the aforementioned solute and ion transporters changed clearly differently in ODMs when compared with data from Caco-2 cells, possibly a reflection of their respective memory of tissue of origin (compare Supplementary Data File 2).

The network analysis suggested that infection triggers overlapping/interdependent, and nonoverlapping/parallel responses. As in the hallmark GSEA, a prominent interdependent subnetwork represented the innate immune response linked to NF-κB/interleukin 1/TNF-α signaling. Annotations of the 40 most highly affected mRNAs (verified also via reverse transcription quantitative polymerase chain reaction; Supplementary Figure S9) revealed this as a major trace. Notably, transcripts of TNF-α showed the largest relative increase due to infection and the whole gene set "TNFA_signaling_via_NFKB" was enriched (Supplementary Figure S10).

Because GSEA suggested changes in apical junctions, we mined the transcriptome data specifically for changed mRNAs encoding TJ proteins (Figure 3G, Supplementary Data File 1). ODMs clearly expressed claudin-1, -2, -3, -4, -7, -12, -15, and -18 (and at very low abundance, claudin-9 and -16 mRNAs), which is the pattern of the small intestine.[22] Apart from claudin-2 ($\sim$16-fold reduced), infection for 24 hours led with high consistency to $\sim$2-fold changes in claudin-1 (reduced) and claudin-4, -7, -12, and -15 (all increased) mRNA abundances. Claudin-3 and -18 mRNA levels were not affected by infection. Overall, this predicted altered TJ channel (related to claudin-2, -7, -12, and -15) and barrier (claudin-1) function. Regarding additional TJ components, such as TJ protein 1 (zonula occludens-1 [ZO-1]) and occludin, relative mRNAs were only 1.4-fold less and 2.7-fold more abundant than in controls, respectively (Figure 3G, Supplementary Data File 1). Some cadherin and nectin genes contributing to desmosomal and adherence junctions were also altered (Supplementary Figure S11).

Reduction of claudin-2 transcription was previously linked to reduced levels of the anion transporter SLC26A3 (DRA).[23] Notably, and as mentioned above, genes of a particular transporter gene set (disease transporter gene set) were broadly and mostly negatively affected (Figure 3F). *SLC26A3* mRNA included in this gene set was $\sim$6-fold reduced by infection. Similarly, mRNAs encoding basolateral *SLC12A2* (*NKCC1*) and apical *CFTR* chloride channels were significantly less abundant compared with their level in controls.

This transcriptional response of ODMs to infection suggests altered ion transport processes preceding changes to TJ properties, the latter resulting in TEER and barrier breakdown. Thus, we aimed at seeking evidence in support of this hypothesis.

Giardia *Infection Reduces Solute Carrier Family 12 Member 2 and Cystic Fibrosis Transmembrane Conductance Regulator-Dependent Chloride Secretion by Human Organoid-Derived Monolayers and Causes Ultrastructural Changes in Tight Junction Network*

Ion secretion was changed early after infection, as captured by monitoring basal I_{SC} (Figure 4A) and prostaglandin E_2/theophylline-stimulated anion secretion (Figure 4B) during infection. Going into detail, infection reduced the SLC12A2 (NKCC1)-specific, hence bumetanide-inhibitable ion transport already early on

Figure 1. Characterization of human intestinal ODMs. (*A*) Duodenal organoids were cultured on transwell filters reaching a plateau of TEER of $\sim$250 $\Omega \cdot cm^2$ after 9 days. (*B*) Orthogonal stacks of representative (immune)-fluorescence assays (IFAs) show F-actin (Phalloidin signal; *top row*) and enterocyte-typical transporter NHE3 (SLC9A3; *bottom row*) at the apical brush border. *Scale bar* = 20 μm. (*C*) Thickness of ODMs over culture time. (*D*) Transmission electron microscopy showing apical contact zone of 2 cells with tight junction (tj), adherens junction (aj), and desmosomes (d). *Scale bar* = 500 nm. (*E*) Phlorizin-inhibitable (sodium–glucose cotransporter 1-dependent) apical glucose uptake. (*F*) Agarose gel of intron spanning polymerase chain reaction fragments corresponding to mRNA of *APOB* and of its processing complex components *APOBEC1* and *A1CF*. (*G*) Western blot showing expression of 2 variants of APOB, APOB-100 and enterocyte specific APOB-48 in ODMs. All quantitative experiments show mean $\pm$ standard error of the mean of at least 7 individual transwell filters of 3 independent experiments. Statistical significance was tested using a 1-way analysis of variance with Tukey's (cell height) or Sidak's (glucose uptake) correction for multiple testing. ****$P < .0001$.
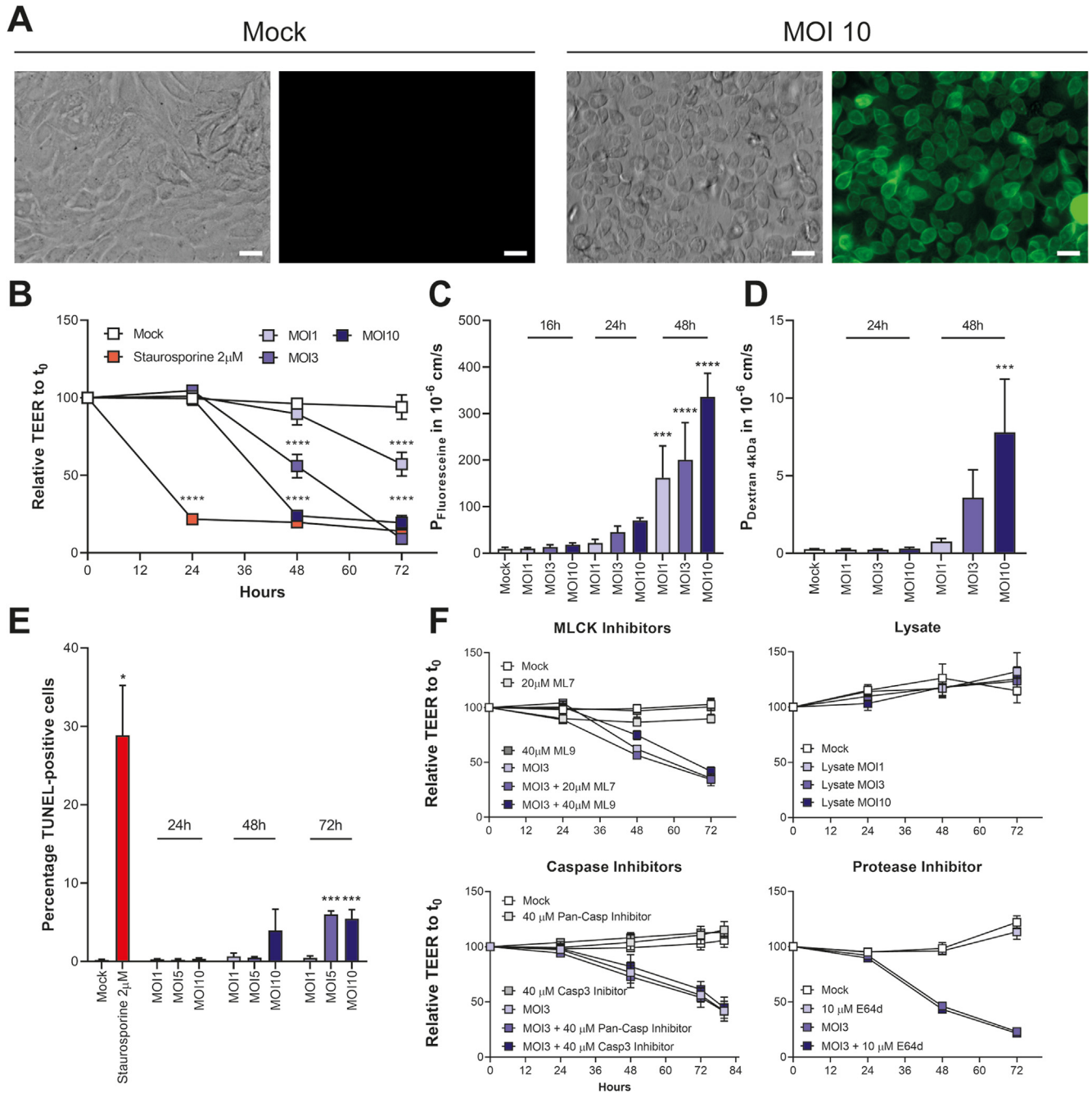
Figure 2. Barrier breakdown of human primary intestinal epithelium after infection with *Giardia* trophozoites. ODMs were infected at different MOI and analyzed at the indicated times. Staurosporine was used to induce apoptosis (positive barrier breakdown control). (*A*) Representative light and fluorescent microscopic images of noninfected ODMs or infected for 2 hours with labeled *Giardia* trophozoites (MOI 10; *green*). *Scale bar* = 20 μm. (*B*) MOI- and time-dependent decrease of TEER after *Giardia* infection. *Giardia*-induced permeability increase for (*C*) fluorescein (332 Da) or (*D*) FD4 (4000 Da). (*E*) MOI- and time-dependent increase of terminal deoxynucleotidyl transferase–mediated deoxyuridine triphosphate nick-end labeling (TUNEL)-positive cells in infected ODMs. Note, MOI 5 instead of 3 was used to illustrate that only with higher parasite doses and longer time points an effect on apoptosis can be detected. (*F*) TEER decrease in ODMs after *Giardia* infection despite treatment with MLCK inhibitors (ML7 and ML9), caspase inhibitors (pan-CASP and CASP3), or cysteine protease inhibitor (E64d). No effect of *Giardia* lysate corresponding to MOI 1, 3, or 10 on TEER in uninfected ODMs. Note, ML9 has been shown to also affect PKA,[43] which explains the partial effect after 48 hours after infection at MOI 3 (see also Figure 6). Differences to untreated conditions were not significant. Quantitation represents mean values $\pm$ standard error of the mean of $\geq$6 individual transwells of $\geq$2 independent experiments. Statistical significance was determined using a 1-way analysis of variance (*C, D, E*) or 2-way analysis of variance (*B, F*) with Dunnett's correction for multiple testing. *P < .05, **P < .01, ***P < .001, ****P < .0001.

BASIC AND
TRANSLATIONAL AT

and clearly at times assessed after 16 hours of infection (Figure 4*C*). Triggering apical Cl⁻ secretion by forskolin and inhibiting CFTR's contribution with 5-nitro-2-(3-phenylpropylamino) benzoic acid (NPPB) revealed reduced CFTR activity in infected ODMs (Figure 4*D*), corroborating the respective mRNA data.
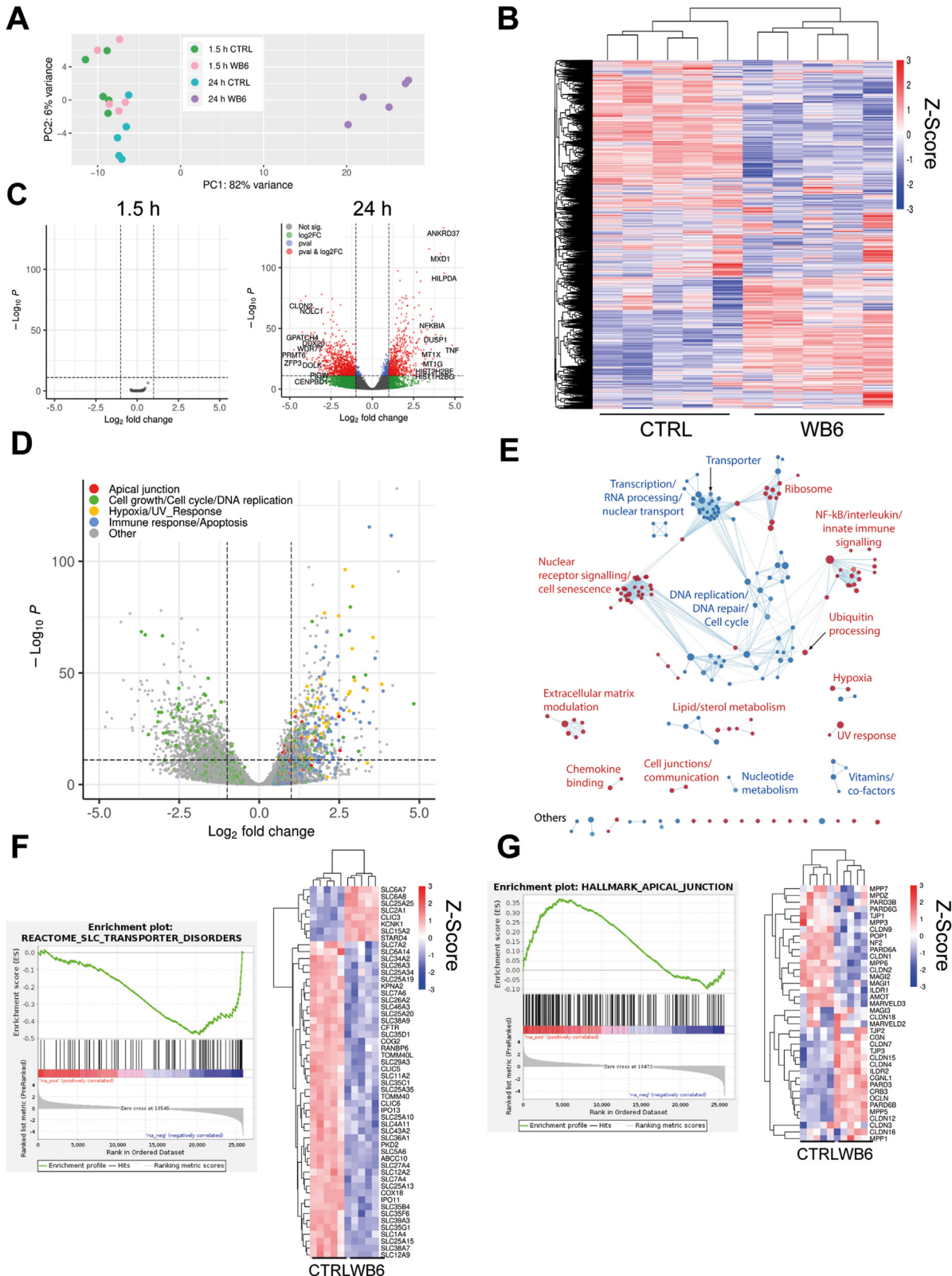
Paracellular ion permeability and charge selectivity were determined next (Figure 4E and F). Uninfected ODMs reproduced the cation-selective TJ properties of the small intestine with a P_{Na}/P_{Cl} ratio of ~ 2 (Figure 4E and F). During infection, permeabilities for ions increased steadily (Figure 4E), and cation selectivity of ODMs was gradually lost as the ratio P_{Na}/P_{Cl} tended more and more toward 1 (Figure 4F). These functional changes corresponded directly to the changes in claudin expression that were found predictive for reduced paracellular barrier function and loss of cation selectivity in other pathologies.[24]

As changes in permeabilities for ions and also for midsize and macromolecular solutes (Figure 2C and D) indicated massive changes in TJ properties, ultrastructural consequences of TJ protein modulation, were assessed. Therefore, we performed freeze-fracture electron microscopy. Infection led to altered TJ ultrastructure and loosening of the TJ meshwork, but this was observed only at 48 hours at MOI 10 (Figure 4G). This was when the paracellular barrier was lost already, corroborating electrophysiological results shown above. Under said conditions, TJ structures were shifted with respect to their position relative to the brush border, and only $\sim 20\%$ of TJs remained located close to the apical microvilli (Supplementary Figure S12). At earlier time points and at lower parasite load, the number of TJ strands, types, and pattern, as well as meshwork depth and localization remained mainly unaltered (Figure 4H, Supplementary Figure S12). In contrast, single strand breaks were significantly induced and increasingly observed from 24 hours after infection (Figure 5I). This indicated early pre-TEER decline modulation of TJ ultrastructural organization.

Infection Alters Tight Junction Composition, Localization, and Structural Organization

The noted structural and functional changes to the TJ may result from altering their components' transcription, protein localization, or processing. Having assessed mRNA levels, we next investigated localization by immunofluorescence (Figure 5A) and protein processing by Western blot analyses of the major TJ proteins (Figure 5B). Consistent with transcriptome data, and extending it, the analysis revealed changes at all mentioned levels but distinctly for individual TJ proteins (Figure 5, Supplementary Figure S13). For example, claudin-1 was early on affected by delocalization and later also at the mRNA level. Claudin-2 was

severely affected from early on by reduced mRNA and then protein levels. Occludin was proteolytically processed while mRNA levels were transiently even increased, maybe as a counterregulatory response. Zonula occludens-1 behaved as claudin-2 but was less severely affected at mRNA and more so at protein level. For claudin-3, -4, -7, -10, -12, and MARVELD2 (tricellulin) mRNA and protein abundance became only reduced in case of claudin-3, -4, and MARVELD2 when TEER values had already declined (ie, MOI 3 and 10 conditions) (Supplementary Figure S13). In summary, TJs became severely affected starting with losing claudin-1 and -2, which is consistent with early reduction in ion selectivity and barrier properties noted above. Interestingly, 48 hours after infection also first proteolytic processing not only of occludin but also of β-actin became detectable at high MOI, indicating a beginning loss of cytoskeletal structural integrity (Figure 5B, Supplementary Figure S13).

Adenosine 3′,5′-Cyclic Monophosphate-Protein Kinase A Pathway as a Driver of Giardia-Induced Barrier Breakdown

Aiming at igniting events leading to TJ changes and TEER breakdown, we reexamined the transcriptome data with a "retrospective" view by asking whether particular transcription factors may be orchestrating the response and point to initial signals. We repeated the GSEA and enrichment network analyses by interrogating the regulatory target gene sets. This revealed overlapping (interconnected) gene sets for 3 transcription factor families: not surprisingly for NF-κB, but also for cAMP response element-binding protein (CREB)/activating transcription factor (ATF) (both associated with up-regulated mRNAs) and E2F (down-regulated mRNAs) families (Figure 6A).

TNF-α signaling via NF-κB was a major signature already in the previous network analysis, and TNF-α had been implicated in TEER loss as well as in intestinal wound healing.[25] Elevated TNF-α secretion upon Giardia infection was confirmed by enzyme-linked immunosorbent assay (Supplementary Figure S10). To probe its relevance, we knocked out TNF-α by clustered regularly interspaced short palindromic repeats (CRISPR)/Cas9 and infected knockout and control ODMs with Giardia. Contrary to expectation, TNF-α was dispensable for TEER breakdown (Figure 6B, Supplementary Figure S10). Also, addition of recombinant TNF-α did not reduce but rather slightly increased TEER in

Figure 3. Giardia alters ODM transcriptome. RNA sequencing was performed in 5 independent replicates per condition at 1.5 and 24 hours after infection (MOI 5). At this time point, MOI barrier integrity was still intact. (A) Principle-component (PC) PC1 and PC2, capturing 82% and 6% of variation respectively, showing differences by PC analysis of protein-coding transcriptional response to Giardia in ODMs at 24 hours after infection. (B) Global heat map (based on Z-scores) of 24-hour infected replicates and respective mock controls. Volcano plots of differential gene expression analysis, mean fold-change vs probability of samples 1.5 hours and 24 hours after infection with (C) respective controls showing in (D) enriched hallmark gene sets (color coded; see also Supplementary Table 3). The dashed lines indicate cutoff values of $\log_2$-fold change (=1) and adjusted P values (10e−12). (E) Network analysis representation of gene sets comprising a customized subset of the curated C2 gene set at MSigDB.org. Interconnected and unconnected groups of nodes were labeled for illustration according to the respective overarching gene sets' function; blue (enriched) or red (depleted). Enrichment plots of (F) sets apical junction and (G) solute carrier (SLC) transporter disorders and respective heat map representation of changes in key transcripts of infected (WB6) vs control (CTRL).
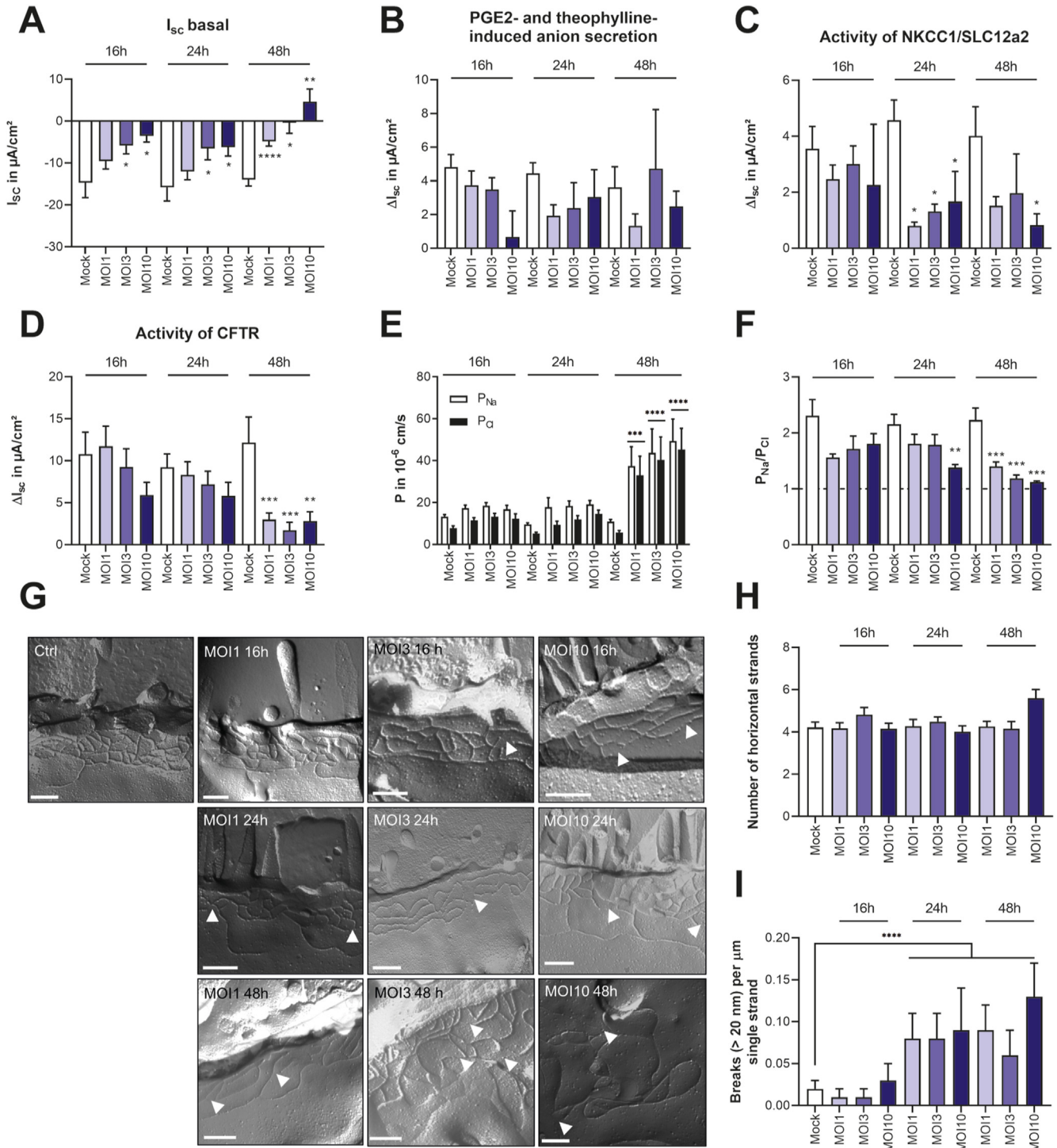
Figure 4. *Giardia*-induced changes in electrophysiology and TJ ultrastructure of ODMs. ODMs were infected at indicated MOI and electrophysiological properties analyzed in Ussing chambers. (*A*) Basal short circuit current (I_{sc}, positive values represent cation absorption/anion secretion) changed MOI and infection time dependently. (*B*) MOI- and time-dependent changes in prostaglandin E_2 (PGE2)- and theophylline-induced anion secretion, and (*C*) specific NKCC1/SLC12a2 and (*D*) CFTR activity. ΔIsc after forskolin treatment was not different between groups at 16 and 24 hours (not shown), but was lower in infected groups after 48 hours (Mock: 16.42 ± 3.22; MOI 1: 3.64 ± 0.87; MOI 3: 2.00 ± 1.07; MOI 10: 4.42 ± 1.14; all in μA/cm^2). (*E*) Permeabilities for sodium (P_{Na}) and chloride (P_{Cl}) of infected ODMs and controls (Mock) at indicated time points. (*F*) Ratio of Na$^+$ and Cl$^-$ permeabilities (P_{Na}/P_{Cl}). (*G*) Representative freeze-fracture electron microscopy images illustrate progressive loss of TJ organization in infected vs noninfected (Mock) ODMs at indicated times. *Arrow heads* illustrate strand breaks. *Scale bar* = 200 nm. (*H*) Enumeration of horizontal strands in TJ complex and (*I*) enumeration of breaks (>20 nm) per μm of TJ strands. *P* values determined using a 2-way analysis of variance with Dunnett's correction for multiple testing. *$P <$ .05, **$P <$ 0.01, ***$P <$ .001, ****$P <$ .0001. Values represent means $\pm$ standard error of the mean of $\geq$5 individual transwell filters of $\geq$2 independent experiments. Freeze-fracture electron microscopy data show mean $\pm$ standard error of the mean of 20–43 TJs assessed per condition.
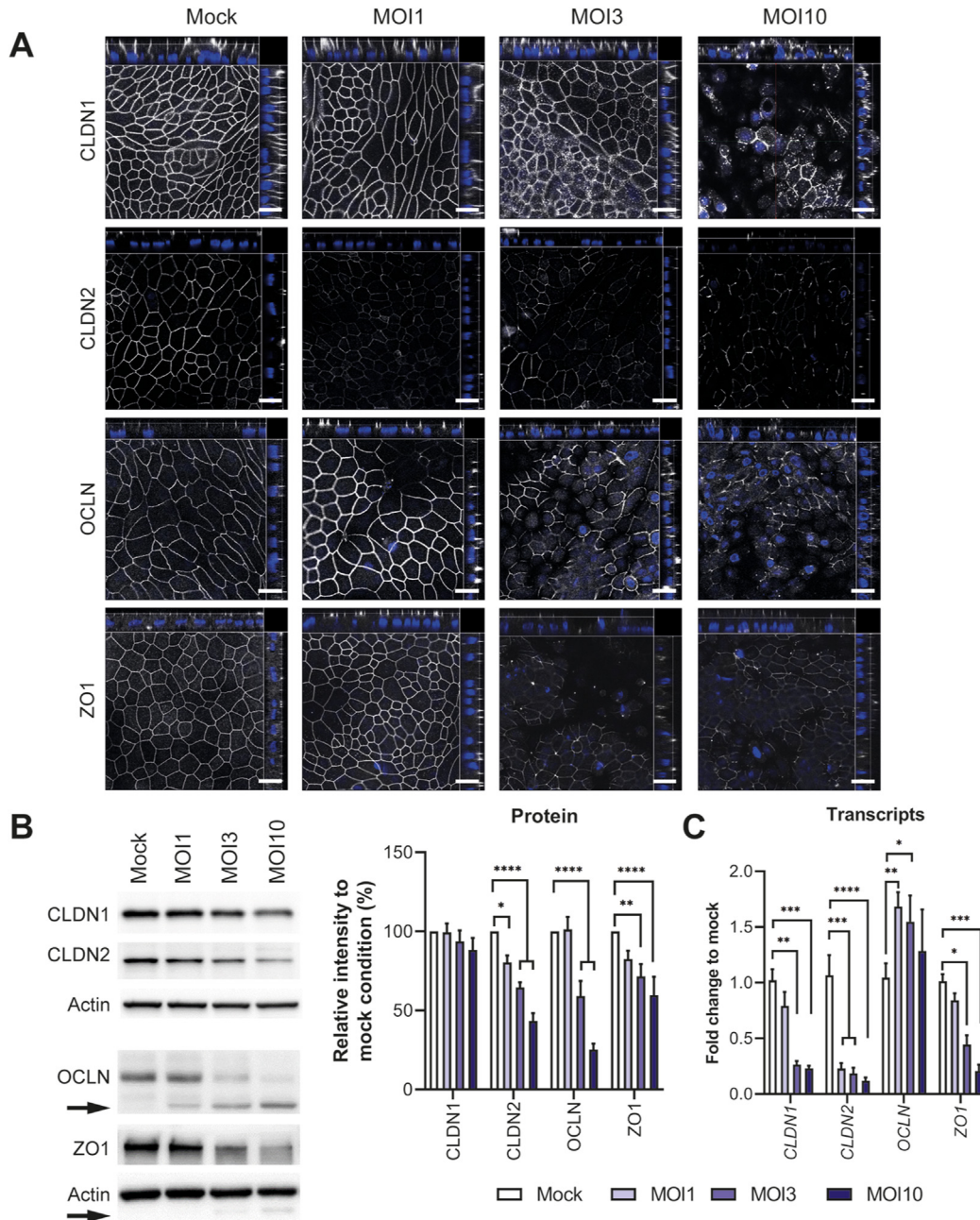
Figure 5. *Giardia*-infection alters TJ protein localization and abundance in ODMs. When TEER values in the MOI 3 sample dropped by 50%, *Giardia* infected ODMs were (*A*) fixed and analyzed by indirect immunofluorescence assay or (*B and C*) used for expression analysis (for images shown at 48 hours; when MOI 1 resulted in no TEER alteration, MOI 10 in complete TEER breakdown). (*A*) Localization of TJ protein 1 (zonula occludens-1 [ZO-1]), claudin-1, claudin-2, and occludin with representative orthogonal stacks of immunofluorescence images, (*B*) protein abundance in Western blot analysis, (*C*) mRNA by quantitative polymerase chain reaction. *Scale bar* $= 20$ μm. Statistical analysis (n $= 6$–8) by a mixed model or 2-way analysis of variance with Dunnett's correction for multiple testing. *$P < .05$, **$P < .01$, ***$P < .001$, ****$P < .0001$.

ODMs, further underlining the observation (Supplementary Figure S10).

Upregulation of E2F target genes, which is indicative of reduced E2F repressor functions,[26] was associated with loss of barrier function in a mouse model for lymphocytic choriomeningitis virus.[27] We therefore did not consider the downregulation of E2F targets in our model to be inducing barrier function breakdown. Accordingly, pharmacologic inhibition of E2F repressor function did not reverse the effect of *Giardia*-induced barrier breakdown; rather, this made the ODMs more prone to barrier leakage (Supplementary Figure S14).

We next followed up on the CREB/ATF family transcriptional signature in response to infection. These transcription factors are regulated by PKA/exchange proteins directly activated by cAMP (EPAC) protein
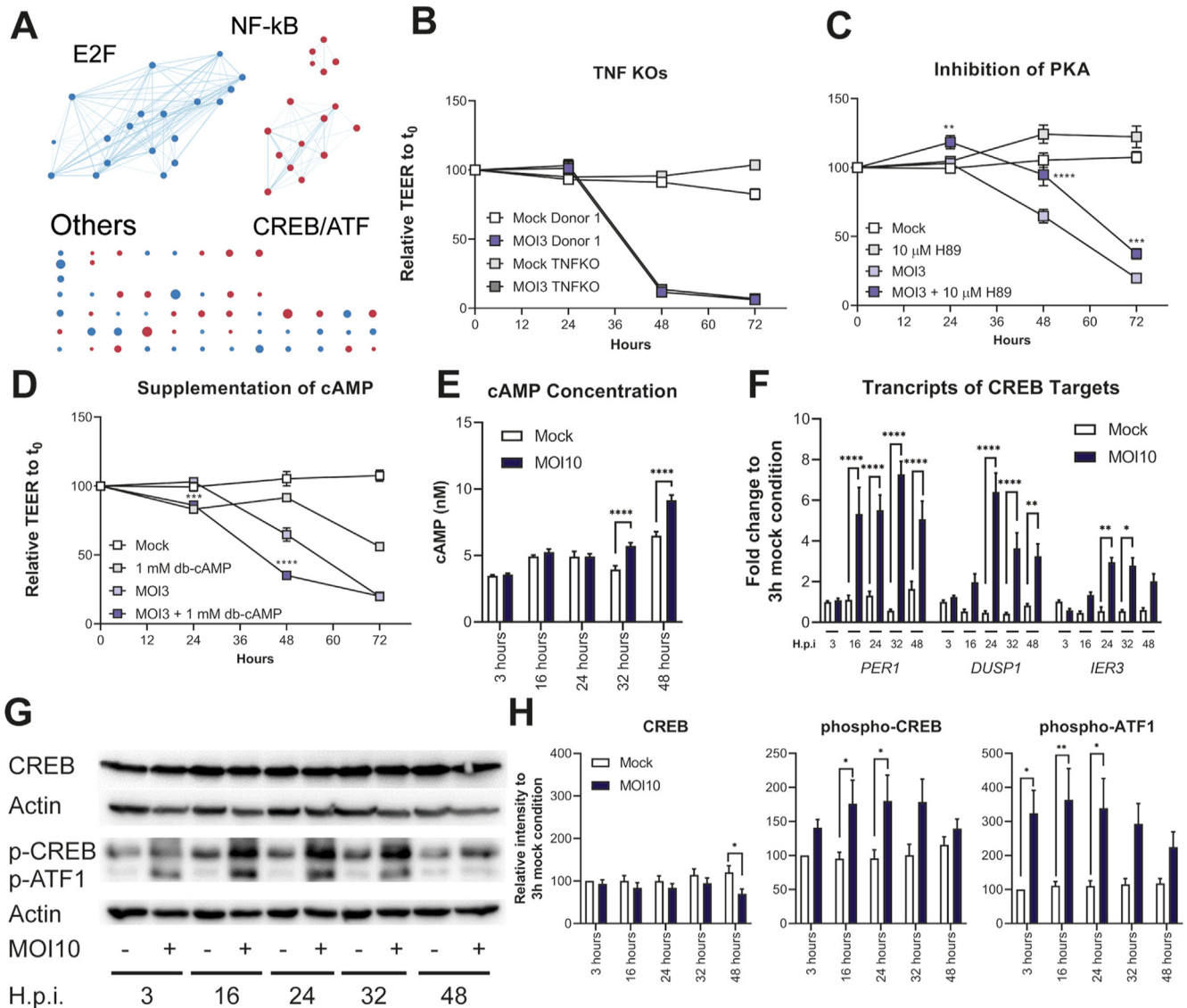
Figure 6. Transcriptome reveals cAMP/PKA-signaling role in *Giardia*-induced TEER breakdown. (*A*) Transcription factor target gene enrichment in *Giardia*-induced transcriptional response of ODM. GSEA and network analysis (see legend Figure 3) using C3 gene sets of MSigDB.org, revealing prominent enrichment (*red*) of NF-κB and CREB/ATF target gene sets and deprivation (*blue*) of E2F target sets in regulated mRNAs. (*B*) Comparison of TEER decrease of TNF-α knockout (TNFKO) and WT (donor 1) ODMs after *Giardia* (MOI 3) or mock infection show that TNF-α is dispensable for *Giardia*-induced TEER breakdown. (*C*) H89-inhibition of PKA attenuating *Giardia*-induced TEER loss and (*D*) cAMP addition exacerbating TEER breakdown. (*E*) Intracellular cAMP concentration is significantly increasing, (*F*, *G*) as is phosphorylation of CREB and ATF-1 protein and (*H*) mRNA transcripts of CREB target genes during the time course of infection compared with uninfected controls. Statistical analysis (n ≥ 6) by a 2-way analysis of variance with Dunnett's (*B–F*) or Tukey's (*G* and *H*) correction for multiple testing. *$P < .05$, **$P < .01$, ***$P < .001$, ****$P < .0001$.

kinases, which are both activated by cAMP.[28] Previously, cAMP/PKA signaling had been suggested to play a role based on data from mouse models of *Giardia* infection[29,30] but had not attracted further attention. Thus, cAMP/PKA signaling may also be relevant for human epithelial cell response to *Giardia*. To test this, we added PKA inhibitor H89 or membrane-permeant dibutyryl-cAMP analogs to our ODM system and monitored TEER decline. Strikingly, H89 partially reversed the effect of *Giardia* and addition of dibutyryl-cAMP exacerbated it (Figure 6*C* and *D*). We confirmed that infection induced accumulation of cAMP (Figure 6*E*) and phosphorylation of CREB/ATF (Figure 6*F–H*) as well as upregulation of known CREB target genes. Since cAMP is an endogenous second messenger in the PKA/EPAC pathway, increasing/inhibiting this pathway in control ODMs should in part mimic *Giardia* infection, which was indeed the case for TEER reduction but not for alteration of TJ protein expression (Supplementary Figure S15). Thus, these findings revealed a significant functional role for cAMP/PKA pathway-dependent mechanisms in *Giardia* infection.

Discussion

Here, an in vitro human duodenal organoid culture system was established to overcome limitations of classical cell lines in revealing deleterious effects of *Giardia* on functionally tight barrier-forming primary epithelia. The parasite caused barrier breakdown but this proceeded independently of previously reported pathways. Instead, a cAMP/PKA pathway dependency was newly identified, contributing early to events culminating in barrier loss.

The pathophysiological correlates of symptomatic giardiasis are not well understood. To date, using intestinal cell line models, TJ disruption and caspase-dependent apoptosis triggered by *Giardia* proteases were thought to ignite barrier breakdown.[1,3,16,18] In one of the very rare clinical studies of patients with chronically symptomatic giardiasis performed by researchers of our group, barrier dysfunction was recognized. At this chronic stage, villus shortening, decreased TEER, increased permeability, altered ion and glucose transport, and increased apoptosis were observed.[6] In agreement with and relevant to our observations, claudin-1 was downregulated and claudin-2 was undetectable.[6] It was concluded that "leak flux, malabsorptive and secretory components" are key factors during chronic giardiasis. Our results are not only in good agreement, but beyond this, also suggest that acute infection triggers a sequence of functionally linked events that lead to these changes with early involvement of cAMP/PKA signaling pathways.

The cAMP/PKA signaling-induced TJ disruption in human intestinal epithelial cells has been shown as a principle reaction pattern of epithelial cells to bacterial toxins (eg, cholera toxin).[31,32] Our observations indicate that the cAMP/PKA-signaling pathway is also a relevant component of *Giardia*'s pathogenic effects. This adds a parasite to the list of the bacterial pathogens *Vibrio cholerae*, *Shigella*, or *Salmonella*, for which induction of diarrhea is known to involve this pathway.[31,32] For cholera toxin, barrier breakdown is proposed to be a consequence of activation of PKA/EPAC, which are thought to inhibit (via an unknown mechanism) the vesicular delivery of proteins to paracellular junctions.[33] Concomitantly, cholera toxin treatment is proposed to lead to PKA-dependent activation of CFTR and Cl^- secretion.[33] While we report PKA signaling-dependent paracellular barrier breakdown, we observed decreased CFTR activity. This discrepancy to cholera toxin's effect is best explained by *Giardia* causing the transcriptional downregulation of *CFTR* already before changes to the TJ occur. Thus, actual net effects on the functional response of epithelia of one and the same signaling pathway are likely different between pathogens, reflecting, among other factors, the kinetics of infection and sequence of events. Reverse genetic tractability of the ODM model by CRISPR/Cas methodology[34] and complementing the approach with genetic manipulation of *Giardia*[35] opens avenues to disentangle these processes at molecular detail in future studies.

A number of studies have indicated defects in ion homeostasis in epithelia after *Giardia* infection.[32,36–38] One, for example, reported decreased CFTR function in cells exposed to parasites or parasite-secreted/released factors.[36] We show that *Giardia* infection alters ion transporter expression and function in epithelial cells before TJ modulation. This sequence of events is in line with reports of altered transporter expression regulating changes in TJ composition and function.[39] We further discovered that TJ changes are observed before cell death contributes to epithelial disintegration.

The result that TNF-α had no effect on TEER breakdown in our model was surprising, because findings in inflammatory diseases, such as inflammatory bowel disease,[40] suggested otherwise. However, the finding is in line with a recent study that highlighted a protective role of TNF-α receptor signaling in epithelial cells.[25] It is therefore worth speculating that autocrine/paracrine TNF-α produced after *Giardia* infection by intestinal epithelia may be one of the not yet known protective factors arming against diarrhea of other etiologies, a feature of giardiasis revealed by epidemiological data (eg, from the Global Enteric Multicenter Study study).[41]

In summary, the presented ODM model suggests a novel sequence of molecular events leading to epithelial barrier breakdown by *Giardia* parasites that adds to understanding of the pathophysiology of giardiasis. Although far-fetched, the findings may justify consideration of antihost response-directed adjunct therapies as an option for difficult-to-treat cases since, for example, interference with cAMP/PKA signaling is pursued in clinical contexts.[42]

Supplementary Material

Note: To access the supplementary material accompanying this article, visit the online version of *Gastroenterology* at www.gastrojournal.org, and at https://dx.doi.org/10.1053/j.gastro.2021.11.022

References

1. Allain T, Buret AG. Pathogenesis and post-infectious complications in giardiasis. Adv Parasitol 2020; 107:173–199.
2. Torgerson PR, Devleesschauwer B, Praet N, et al. World Health Organization estimates of the global and regional disease burden of 11 foodborne parasitic diseases, 2010: a data synthesis. PLoS Med 2015;12:e1001920.
3. Einarsson E, Ma'ayeh S, Svard SG. An up-date on *Giardia* and giardiasis. Curr Opin Microbiol 2016; 34:47–52.
4. Oberhuber G, Kastner N, Stolte M. Giardiasis: a histologic analysis of 567 cases. Scand J Gastroenterol 1997; 32:48–51.
5. Pham JK, Nosala C, Scott EY, et al. Transcriptomic profiling of high-density *Giardia* foci encysting in the

murine proximal intestine. Front Cell Infect Microbiol 2017;7:227.

6. Troeger H, Epple HJ, Schneider T, et al. Effect of chronic *Giardia lamblia* infection on epithelial transport and barrier function in human duodenum. Gut 2007;56:328–335.

7. Kraft MR, Klotz C, Bucker R, et al. *Giardia*'s epithelial cell interaction in vitro: mimicking asymptomatic infection? Front Cell Infect Microbiol 2017;7:421.

8. **Kraiczy J, Nayak KM**, Howell KJ, et al. DNA methylation defines regional identity of human intestinal epithelial organoids and undergoes dynamic changes during development. Gut 2019;68:49–61.

9. Tokuhara Y, Morinishi T, Matsunaga T, et al. Nuclear expression of claudin-3 in human colorectal adenocarcinoma cell lines and tissues. Oncol Lett 2018;15:99–108.

10. Nash TE. Long-term culture of *Giardia lamblia* in cell culture medium requires intimate association with viable mammalian cells. Infect Immun 2019;87:e00639-1.

11. Bartfeld S. Modeling infectious diseases and host-microbe interactions in gastrointestinal organoids. Dev Biol 2016;420:262–270.

12. Sato T, Stange DE, Ferrante M, et al. Long-term expansion of epithelial organoids from human colon, adenoma, adenocarcinoma, and Barrett's epithelium. Gastroenterology 2011;141:1762–1772.

13. VanDussen KL, Marinshaw JM, Shaikh N, et al. Development of an enhanced human gastrointestinal epithelial culture system to facilitate patient-based assays. Gut 2015;64:911–920.

14. Keister DB. Axenic culture of *Giardia lamblia* in TYI-S-33 medium supplemented with bile. Trans R Soc Trop Med Hyg 1983;77:487–488.

15. Yu ASL. Electrophysiological characterization of claudin ion permeability using stably transfected epithelial cell lines. Claudins 2011;762:27–41.

16. Chin AC, Teoh DA, Scott KGE, et al. Strain-dependent induction of enterocyte apoptosis by *Giardia lamblia* disrupts epithelial barrier function in a caspase-3-dependent manner. Infect Immun 2002;70:3673–3680.

17. Liu J, Ma'ayeh S, Peirasmaki D, et al. Secreted *Giardia intestinalis* cysteine proteases disrupt intestinal epithelial cell junctional complexes and degrade chemokines. Virulence 2018;9:879–894.

18. Scott KG, Meddings JB, Kirk DR, et al. Intestinal infection with *Giardia* spp. reduces epithelial barrier function in a myosin light chain kinase-dependent fashion. Gastroenterology 2002;123:1179–1190.

19. **Subramanian A, Tamayo P**, Mootha VK, et al. Gene set enrichment analysis: a knowledge-based approach for interpreting genome-wide expression profiles. Proc Natl Acad Sci U S A 2005;102:15545–15550.

20. Ma'ayeh SY, Knorr L, Skold K, et al. Responses of the differentiated intestinal epithelial cell line Caco-2 to infection with the *Giardia intestinalis* GS isolate. Front Cell Infect Microbiol 2018;8:244.

21. Roxstrom-Lindquist K, Ringqvist E, Palm D, et al. *Giardia lamblia*-induced changes in gene expression in differentiated Caco-2 human intestinal epithelial cells. Infect Immun 2005;73:8204–8208.

22. Luettig J, Rosenthal R, Barmeyer C, et al. Claudin-2 as a mediator of leaky gut barrier during intestinal inflammation. Tissue Barriers 2015;3:e977176.

23. Balkovetz DF, Chumley P, Amlal H. Downregulation of claudin-2 expression in renal epithelial cells by metabolic acidosis. Am J Physiol Renal Physiol 2009;297:F604–F611.

24. Krug SM, Schulzke JD, Fromm M. Tight junction, selective permeability, and related diseases. Semin Cell Dev Biol 2014;36:166–176.

25. **Bradford EM, Ryu SH**, Singh AP, et al. Epithelial TNF receptor signaling promotes mucosal repair in inflammatory bowel disease. J Immunol 2017; 199:1886–1897.

26. Kurtyka CA, Chen L, Cress WD. E2F inhibition synergizes with paclitaxel in lung cancer cell lines. PLoS One 2014;9:e96357.

27. Labarta-Bajo L, Nilsen SP, Humphrey G, et al. Type I IFNs and CD8 T cells increase intestinal barrier permeability after chronic viral infection. J Exp Med 2020;217: e20192276.

28. Cheng X, Ji Z, Tsalkova T, et al. Epac and PKA: a tale of two intracellular cAMP receptors. Acta Biochim Biophys Sin (Shanghai) 2008;40:651–662.

29. Ganguly NK, Mahajan RC, Radhakrishna V, et al. Effect of *Giardia lamblia* infection on the intestinal cyclic AMP level in mice. J Diarrhoeal Dis Res 1984;2:69–72.

30. Shant J, Ghosh S, Bhattacharyya S, et al. The alteration in signal transduction parameters induced by the excretory-secretory product from *Giardia lamblia*. Parasitology 2004;129:421–430.

31. Camilleri M, Sellin JH, Barrett KE. Pathophysiology, evaluation, and management of chronic watery diarrhea. Gastroenterology 2017;152:515–532 e2.

32. **Hodges K, Gill R**. Infectious diarrhea: cellular and molecular mechanisms. Gut Microbes 2010;1:4–21.

33. Guichard A, Cruz-Moreno B, Aguilar B, et al. Cholera toxin disrupts barrier function by inhibiting exocyst-mediated trafficking of host proteins to intestinal cell junctions. Cell Host Microbe 2013;14:294–305.

34. Ringel T, Frey N, Ringnalda F, et al. Genome-scale CRISPR screening in human intestinal organoids identifies drivers of TGF-beta resistance. Cell Stem Cell 2020;26:431–440.e8.

35. **McInally SG, Hagen KD**, Nosala C, et al. Robust and stable transcriptional repression in Giardia using CRISPRi. Mol Biol Cell 2018mbcE18090605.

36. Dubourg A, Xia D, Winpenny JP, et al. *Giardia* secretome highlights secreted tenascins as a key component of pathogenesis. Gigascience 2018;7:1–13.

37. Gorowara S, Ganguly NK, Mahajan RC, et al. Role of calcium and calmodulin in *Giardia lamblia*-induced diarrhoea in mice. J Diarrhoeal Dis Res 1991;9:111–117.

38. Gorowara S, Ganguly NK, Mahajan RC, et al. Study on the mechanism of *Giardia lamblia* induced diarrhoea in mice. Biochim Biophys Acta 1992;1138:122–126.

39. Rajasekaran SA, Palmer LG, Moon SY, et al. Na,K-ATPase activity is required for formation of tight

BASIC AND TRANSLATIONAL AT

junctions, desmosomes, and induction of polarity in epithelial cells. Mol Biol Cell 2001;12:3717–3732.

40. Amoozadeh Y, Dan Q, Xiao J, et al. Tumor necrosis factor-alpha induces a biphasic change in claudin-2 expression in tubular epithelial cells: role in barrier functions. Am J Physiol Cell Physiol 2015;309:C38–C50.

41. Kotloff KL, Nasrin D, Blackwelder WC, et al. The incidence, aetiology, and adverse clinical consequences of less severe diarrhoeal episodes among infants and children residing in low-income and middle-income countries: a 12-month case-control study as a follow-on to the Global Enteric Multicenter Study (GEMS). Lancet Glob Health 2019;7:e568–e584.

42. Raker VK, Becker C, Steinbrink K. The cAMP pathway as therapeutic target in autoimmune and inflammatory diseases. Front Immunol 2016;7:123.

43. Saitoh M, Ishikawa T, Matsushima S, et al. Selective inhibition of catalytic activity of smooth muscle myosin light chain kinase. J Biol Chem 1987;262:7796–7801.

Author names in bold designate shared co-first authorship.

Correspondence
Address correspondence to: Christian Klotz, PhD, Department of Infectious Diseases, Unit 16 Mycotic and Parasitic Agents and Mycobacteria, Robert Koch-Institute, Seestraße 10, 13353 Berlin, Germany. e-mail: klotzc@rki.de.

Data Availability
All data are available in the original manuscript and online Supplementary Material.

CRediT Authorship Contributions
David Holthaus, MSc (Conceptualization: Equal; Data curation: Equal; Formal analysis: Equal; Investigation: Equal; Methodology: Equal; Visualization: Equal; Writing – original draft: Equal; Writing – review & editing: Equal). Martin Kraft, PhD (Conceptualization: Equal; Data curation: Equal; Formal analysis: Equal; Investigation: Equal; Methodology: Equal; Visualization: Equal; Writing – review & editing: Equal). Susanne M. Krug, PhD (Conceptualization: Supporting; Data curation: Equal; Formal analysis: Supporting; Investigation: Supporting; Methodology: Supporting; Visualization: Supporting; Writing – original draft: Supporting; Writing – review & editing: Supporting). Silver Wolf, MSc (Data curation: Supporting; Formal analysis: Supporting; Investigation: Supporting; Methodology: Supporting; Software: Supporting; Visualization: Supporting; Writing – review & editing: Supporting). Antonia Müller, MSc (Formal analysis: Supporting; Investigation: Supporting; Methodology: Supporting; Writing – review & editing: Supporting). Estefania Delgado Betancourt, MSc (Investigation: Supporting; Methodology: Supporting; Visualization: Supporting; Writing – review & editing: Supporting). Madeleine Schorr, MSc (Investigation: Supporting; Methodology: Supporting; Writing – review & editing: Supporting). Gudrun Holland, MSc (Data curation: Supporting; Formal analysis: Supporting; Investigation: Supporting; Methodology: Supporting; Visualization: Supporting). Felix Knauf, MD (Resources: Supporting; Writing – review & editing: Supporting). Joerg-Dieter Schulzke, MD (Data curation: Supporting; Formal analysis: Supporting; Resources: Supporting; Writing – review & editing: Supporting). Toni Aebischer, PhD (Conceptualization: Lead; Data curation: Equal; Formal analysis: Equal; Funding acquisition: Equal; Visualization: Supporting; Writing – original draft: Lead; Writing – review & editing: Lead). Christian Klotz, PhD (Conceptualization: Lead; Data curation: Equal; Formal analysis: Equal; Investigation: Equal; Methodology: Equal; Resources: Equal; Visualization: Equal; Writing – original draft: Lead; Writing – review & editing: Lead).